Infragravity-Frequency (0.005–0.05 Hz) Motions on the Shelf. Part II: Free Waves

T. H. C. HERBERS

Department of Oceanography, Naval Postgraduate School, Monterey, California

STEVE ELGAR

School of Electrical Engineering and Computer Science, Washington State University, Pullman, Washington

R. T. GUZA AND W. C. O'REILLY

Center for Coastal Studies, Scripps Institution of Oceanography, La Jolla, California

(Manuscript received 11 January 1994, in final form 14 July 1994)

ABSTRACT

In Part I, the energy levels of ocean surface waves at infragravity frequencies (nominally 0.005–0.05 Hz) locally forced by swell in 13-m water depth were shown to be predicted accurately by second-order nonlinear wave theory. However, forced infragravity waves were consistently much less energetic than free infragravity waves. Here, in Part II, observations in depths between 8 and 204 m, on Atlantic and Pacific shelves, are used to investigate the sources and variability of free infragravity wave energy. Both free and forced infragravity energy levels generally increase with increasing swell energy and decreasing water depth, but their dependencies are markedly different. Although free waves usually dominate the infragravity frequency band, forced waves contribute a significant fraction of the total infragravity energy with high energy swell and/or in very shallow water. The observed h^{-1} variation of free infragravity energy with increasing water depth h is stronger than the $h^{-1/2}$ dependence predicted for leaky surface gravity waves propagating approximately perpendicular to local depth contours, but is consistent with a heuristic, geometrical optics-based (WKB) model of the refractive trapping of a directionally broad wave field generated close to shore. Preliminary analysis shows that free infragravity waves are indeed directionally broad and that the propagation directions of infragravity waves and incident swell are related. Free infragravity energy levels also depend on the general geographic surroundings. Comparisons of observations from the same depth and with similar swell conditions, but on different shelves, suggest that more free infragravity wave energy is radiated from wide, sandy beaches than from rocky, cliffed coasts and that less energy is trapped on a narrow shelf than on a wide shelf.

1. Introduction

Waves with infragravity periods (about 0.5–5 min), slightly longer than the periods of wind-generated sea and swell waves (typically 2–20 sec), can be very energetic close to shore with surface elevation variances $O(10^3\ \text{cm}^2)$ (Holman et al. 1978; Wright et al. 1982; Guza and Thornton 1985). Although high correlations observed between infragravity and wind wave energy levels suggest that infragravity waves are driven by wind waves (e.g., Munk 1949; Tucker 1950; Holman et al. 1978; Okihiro et al. 1992; Elgar et al. 1992; and others), the precise generation mechanisms are not well understood.

Nonlinear interaction between two wind wave components with slightly different frequencies f and $f + \Delta f$ theoretically excites a forced secondary wave with a relatively low (infragravity) frequency Δf (Longuet-Higgins and Stewart 1962; Hasselmann 1962). The forced wave energy theoretically depends on the directions of the interacting waves, as well as on their energy and frequency. In Part I of this study (Herbers et al. 1994, hereafter referred to as Part I) estimates of the frequency–directional spectrum of swell and sea obtained from an array of bottom-mounted pressure transducers deployed in 13-m depth, 2 km from shore were used to predict accurately forced infragravity wave properties. Bispectral analysis (e.g., Hasselmann et al. 1963) was used to decompose the observed infragravity waves into forced waves, which are phase coupled to swell and sea, and other uncoupled motions. Although observed and predicted spectra of forced bottom-pressure fluctuations were in good agreement, the observed total (i.e., coupled plus uncoupled) infragravity spectral levels were between 3 and 1500 times higher than the forced infragravity levels, indicating that the infragravity band was often dominated by free, uncoupled mo-

Corresponding author address: Dr. Thomas H. C. Herbers, Department of Oceanography, Code OC/He, Naval Postgraduate School, Monterey, CA 93943-5122.
E-mail: herbers@oc.nps.navy.mil

tions (consistent with earlier studies: Okihiro et al. 1992; Elgar et al. 1992). The present study (Part II) focuses on free, uncoupled infragravity motions.

Longuet-Higgins and Stewart (1962) suggested, based on observations by Munk (1949) and Tucker (1950), that as incident wind waves are dissipated by breaking in very shallow water, shoreward propagating forced infragravity waves are somehow released as free waves, reflected from the beach, and radiated seaward. Subsequently, idealized models describing the generation of leaky (radiating out to deep water) and edge waves at infragravity frequencies through nonlinear interactions and breaking of surface gravity waves have been developed (e.g., Gallagher 1971; Bowen and Guza 1978; Foda and Mei 1981; Symonds et al. 1982; Schäffer and Svendsen 1988; Schäffer et al. 1990; List 1992; Roelvink et al. 1992; Schäffer 1993; and others), but the processes controlling the variability of free infragravity waves on natural beaches are still poorly understood. Alongshore wavenumber spectra of infragravity motions in a few meters depth indicate that a significant fraction of the seaward radiated infragravity energy is refractively trapped as edge waves within a few hundred meters of the shoreline (Huntley et al. 1981; Oltman-Shay and Guza 1987; Howd et al. 1991). Observed variations in infragravity energy on the continental shelf (Okihiro et al. 1992) and weak infragravity energy levels measured in the deep ocean (Webb et al. 1991) are consistent with continued effective refractive trapping across the entire shelf.

Whereas forced wave energy levels are a function only of the local wave field and water depth (see Part I), free wave energy levels may also depend on the topography of nearby shores and the surrounding shelf. In the present study, long-term bottom-pressure measurements (described in section 2) collected in depths ranging from 8 to 204 m, including sites near and far from shore, on broad (North Carolina and Virginia) and narrow (California and Hawaii) shelves, and offshore of both gently sloping beaches and steep rocky cliffs are compared and contrasted. The dependence of free and forced waves on the water depth and local swell conditions is discussed in section 3, where it is shown that refractive trapping controls the cross-shore distribution of free infragravity wave energy. It is also shown that the observed broad directional distributions of infragravity wave energy vary in response to changes in incident swell propagation directions. In section 4, a geometrical optics-based (WKB) model for the propagation of long waves asymptotically far from shore is shown to predict qualitatively the observed depth dependence and broad directional spread of free infragravity wave energy. The sensitivity of infragravity energy levels to surrounding shelf and beach topography is illustrated in section 5 by comparing observations made in the same depth at different sites. In section 6 it is shown that when local swell energy levels are extremely low, the infragravity wave field is dominated by arrivals from remote (possibly transoceanic) sources. The results are summarized in section 7.

2. Field data

Infragravity motions on the shelf were investigated with observations from Atlantic and Pacific sites (Fig. 1). Nine months of bottom pressure data (September 1990–May 1991) were collected in 8-m and 13-m depths on the broad (about 80 km wide) North Carolina shelf, approximately 1 and 2 km offshore of Duck, respectively [Figs. 1a and 2; see Elgar et al. (1992) and Part I for experimental details]. One month of bottom pressure data was obtained in the fall of 1988 at the Chesapeake Light Tower situated in 13-m depth on a shoal about 25 km offshore of the Chesapeake Bay mouth (Figs. 1a and 2; Herbers and Guza 1991). Other field sites were on the much narrower shelves of Hawaii and California. An approximately yearlong bottom pressure record was collected 1 km from shore in 8-m depth at Oahu, Hawaii, where the shelf is less than 2 km wide (Figs. 1c and 2; Okihiro et al. 1992). Three-month long bottom pressure records in 30-m depth were collected during fall/winter of 1991/92 at 16 locations along the southern California coast and at four locations around Santa Rosa, a rocky island in the Southern California Bight with steep cliffs and shallow reefs (O'Reilly et al. 1992). Two representative coastal sites offshore of sandy beaches (Ventura and Redondo) and one of the Santa Rosa rocky island stations are discussed here (Fig. 1b). Measurements in 204-m depth were obtained during six months in the fall/winter of 1991/92 from a pressure gauge mounted 16 m below the sea surface on Harvest Platform, located at the edge of the California shelf (Fig. 1b; Seymour et al. 1985).

The pressure data (sample rates between 0.5 and 4 Hz) were divided into 170-min long records (137 min when longer continuous records were not available). Pressure spectra with 0.0005-Hz resolution (obtained from overlapped, detided, and tapered 34-min segments) were converted to sea surface elevation with the depth correction of linear theory (the correction is negligible at infragravity frequencies). Differences in the wind wave climate, particularly between Pacific and Atlantic Ocean sites are apparent in the average spectral shapes above 0.04 Hz (Fig. 3a). The trend of decreasing relative spectral levels at infragravity frequencies with increasing water depth is qualitatively consistent with the theoretical depth-dependence of forced waves and/or the refractive trapping of free waves (e.g., Okihiro et al. 1992).

Local maxima in the infragravity spectra occur at the frequencies of standing wave antinodes associated with shoreline reflections (e.g., Suhayda 1974), especially in the 8-m and 13-m depth data collected close to shore (Fig. 3a). In deeper water, farther from shore, phase coupling between seaward and shoreward propagating waves is not resolved owing to the reduced fre-

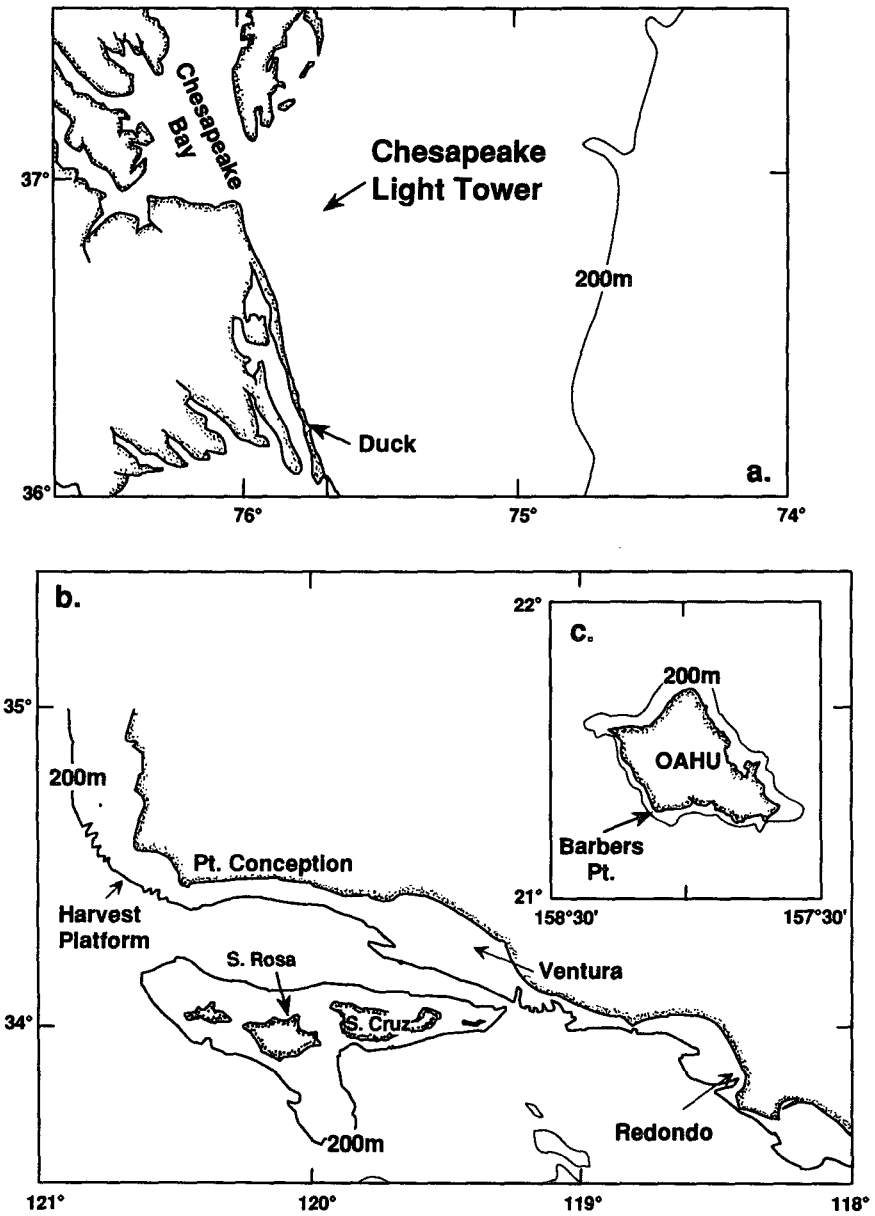

FIG. 1. Locations of pressure measurements: depths (a) 8 m (Duck) and 13 m (Duck and the Chesapeake Light Tower) on the North Carolina/Virginia shelf, (b) 30 m (Redondo, Ventura, and Santa Rosa Island) and 204 m (Harvest Platform) on the California shelf, and (c) 8 m at Oahu, Hawaii. The shelf break corresponds approximately to the 200-m depth contour.

quency separation of nodes and antinodes and possibly directional spreading effects. In the results presented below, standing wave effects are further reduced by averaging the infragravity spectra across a wide frequency bandwidth. Standing wave nodes and antinodes cancel in these smoothed spectra and, thus, measured spectral levels (i.e., bottom pressure variance including free and forced waves) are approximately linearly proportional to the infragravity wave energy [see Hasselmann (1962), Okihiro et al. (1992), and Part I for further discussion of secondary wave energy]. Observed spectra will therefore be referred to as "energy spectra."

At all sites, the observed spectral density at infragravity frequencies and the total swell energy are highly correlated (correlation coefficients above 0.6 in the band 0.004–0.04 Hz, Fig. 3b). Correlations drop rapidly at frequencies above about 0.04 and 0.05 Hz at the Pacific and Atlantic sites, respectively, probably owing to very low-frequency swells from distant storms that are statistically independent of the dominant

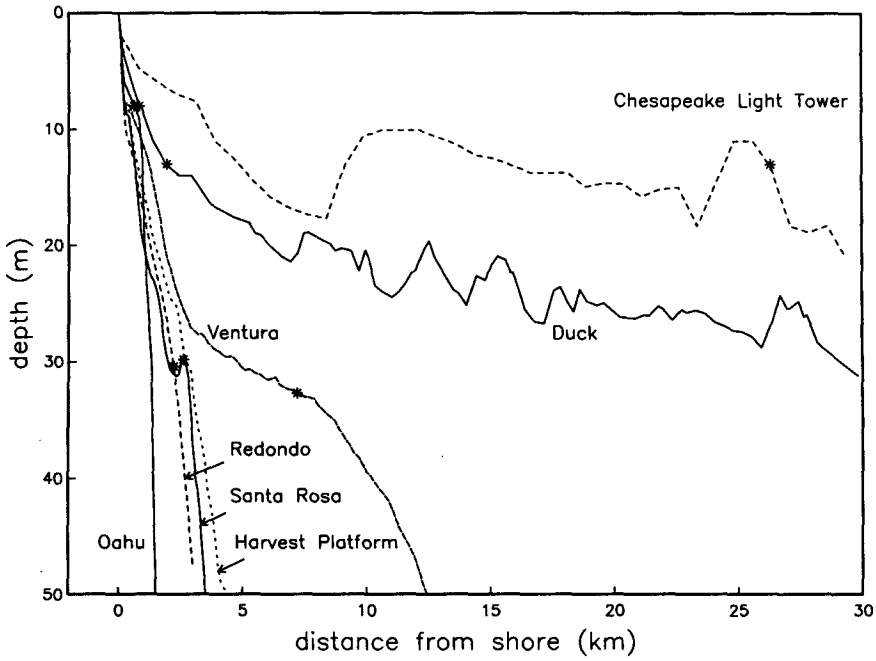

FIG. 2. Cross-shelf depth variations at the field sites. Asterisks indicate pressure gauge locations.

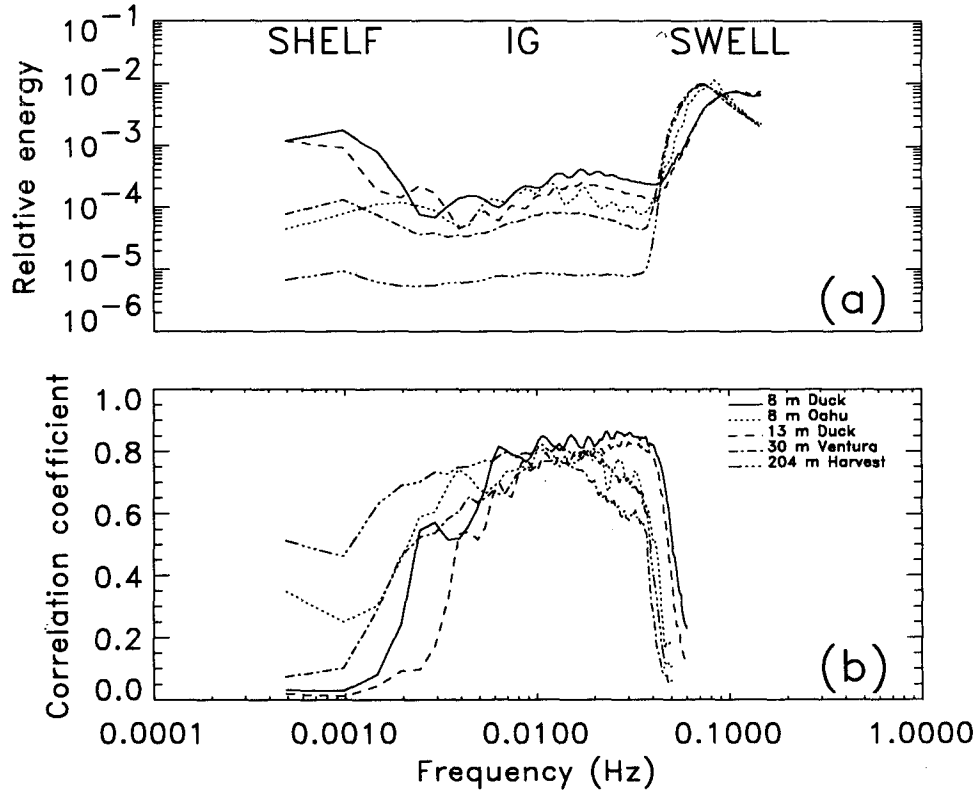

FIG. 3. (a) Average spectral shapes (the average of spectra normalized by the variance in the frequency range 0.0005–0.14 Hz). (b) Observed correlation between the logarithms of spectral levels in narrow (0.0005 Hz wide) frequency bands and total swell energy, as a function of frequency. The total swell energy is equal to the surface elevation spectrum integrated over the frequency range 0.05–0.14 Hz in the Atlantic and 0.04–0.14 Hz in the Pacific.

swells. The correlations also fall off below about 0.004 Hz (Fig. 3b), indicating that motions at lower frequencies were not generated by swell, consistent with earlier studies (e.g., Munk et al. 1956; Morison and Imberger 1992). Relatively little is known about these 5–30-min oscillations. Munk et al. (1956) suggest they are edge waves excited by atmospheric pressure fluctuations (see also Greenspan 1956; Shillington and van Foreest 1986; Evans 1988) or by tsunamis impinging on the shelf, but observational evidence is still scarce (e.g., Snodgrass et al. 1962; Miller et al. 1962; Beardsley et al. 1977; Shillington 1984; Van Dorn 1984). Recently, Giese et al. (1990) and Chapman and Giese (1990) showed that internal waves associated with large amplitude tides generate energetic sea level fluctuations with periods of about 50 min on the Puerto Rican shelf. A transition between infragravity motions (driven by swell) and lower-frequency shelf motions (forced by other mechanisms) is particularly evident on the broad shelf at Duck, where the correlation with swell energy drops off sharply below about 0.002 Hz (Fig. 3b) while the spectral density increases (Fig. 3a). In contrast, on narrower shelves (e.g., 8 m Oahu and 204 m Harvest, Figs. 1 and 2) the spectral levels below 0.002 Hz are relatively low (Fig. 3a) and high correlations with swell energy extend to periods as long as 30 min (Fig. 3b).

Because the present study concerns infragravity motions generated by swell, frequencies below 0.004 Hz (where the correlation with swell energy is sometimes weak, Fig. 3b) are not considered. To avoid contamination of the estimated infragravity wave energy levels by very low frequency swells arriving from distant storms, the upper frequency limit of the infragravity band was chosen to be 0.05 and 0.04 Hz for observations in the Atlantic and Pacific, respectively.

3. Variability of forced and free infragravity energy

Contributions of forced waves, locally excited by nonlinear wave–wave interactions, to the total observed infragravity energy were estimated with bispectral analysis (frequency domain analysis of third-order statistics, Hasselmann et al. 1963). The technique, based on double integration of bispectra over all possible pairs of waves with a difference frequency in the infragravity band, yields estimates of the infragravity band-integrated forced wave energy (see Part I). Interactions of the dominant wind waves (0.04–0.2 Hz in the Pacific, 0.05–0.2 Hz in the Atlantic) were included in these calculations. Errors are introduced in the forced wave energy estimates by directional spreading of the swell, statistical uncertainty in the bispectra, and possibly phase coupling between shoreward propagating swell and seaward propagating free infragravity waves. It was shown in Part I that errors from the first source are usually small. Errors from the latter two sources are greatly reduced by integration over the infragravity frequency band. Bispectrum-based estimates of the energy and phase (relative to the interacting swells) of forced waves observed in 13-m depth at Duck were shown in Part I to be in good agreement with predictions of second-order theory for weakly nonlinear waves. Similar phase results (not shown) were obtained for the present datasets, even though in a few cases the nonlinearity may not have been particularly weak (i.e., the 8-m depth gauges were within the surf zone on some occasions, and significant wave heights occasionally exceeded 6 m at Harvest Platform).

Forced and free infragravity wave energies observed in depths 8, 30, and 204 m are compared in Fig. 4. In all three depths forced wave energy is approximately proportional to the swell energy squared (Fig. 4a), as predicted by second-order nonlinear theory. Since the coupling coefficient relating infragravity and swell energies depends on the details of the swell frequency–directional spectrum, as well as the depth, scatter about a line with slope 2 is expected. In 204-m depth the observed forced wave energy levels are typically a factor of 10^2–10^3 smaller than in 8-m depth for the same swell energy, qualitatively consistent with the theoretical rapid decrease of forced wave energy with increasing water depth (Longuet-Higgins and Stewart 1962; Hasselmann 1962).

The more gradual decrease of free infragravity energy with increasing depth (Fig. 4b) possibly results from unshoaling and refractive trapping of seaward propagating free waves generated close to shore (Okihiro et al. 1992). In contrast to the quadratic dependence of forced wave energy on swell energy, free wave energy is approximately linearly proportional to swell energy (Fig. 4b and all other sites investigated). The observed weaker dependence of free infragravity energy on swell energy is not necessarily inconsistent with nonlinear generation at nearby shores, but suggests that wave breaking is important in the generation process. If the source of free infragravity energy was forced waves released at a fixed location close to shore, then both free and forced infragravity energy should be roughly proportional to the square of the swell energy. However, if the nonlinear transfer of energy to low frequencies is arrested when the swell energy is dissipated through wave breaking, then (because larger amplitude swells break farther from shore) the dependence of free infragravity energy released at the breakpoint on incident swell energy will be weaker than quadratic (Longuet-Higgins and Stewart 1962). Alternative models (e.g., Symonds et al. 1982), which assume that free infragravity waves are driven by variations in setup inside the surf zone rather than nonlinear interactions outside the surf zone, also predict a weaker than quadratic dependence on swell energy, qualitatively consistent with the present observations. The considerable scatter about the trend suggests that free infragravity energy levels on the shelf may be sensitive to the swell frequency–directional spectrum, as is the case for forced waves (Fig. 4a).

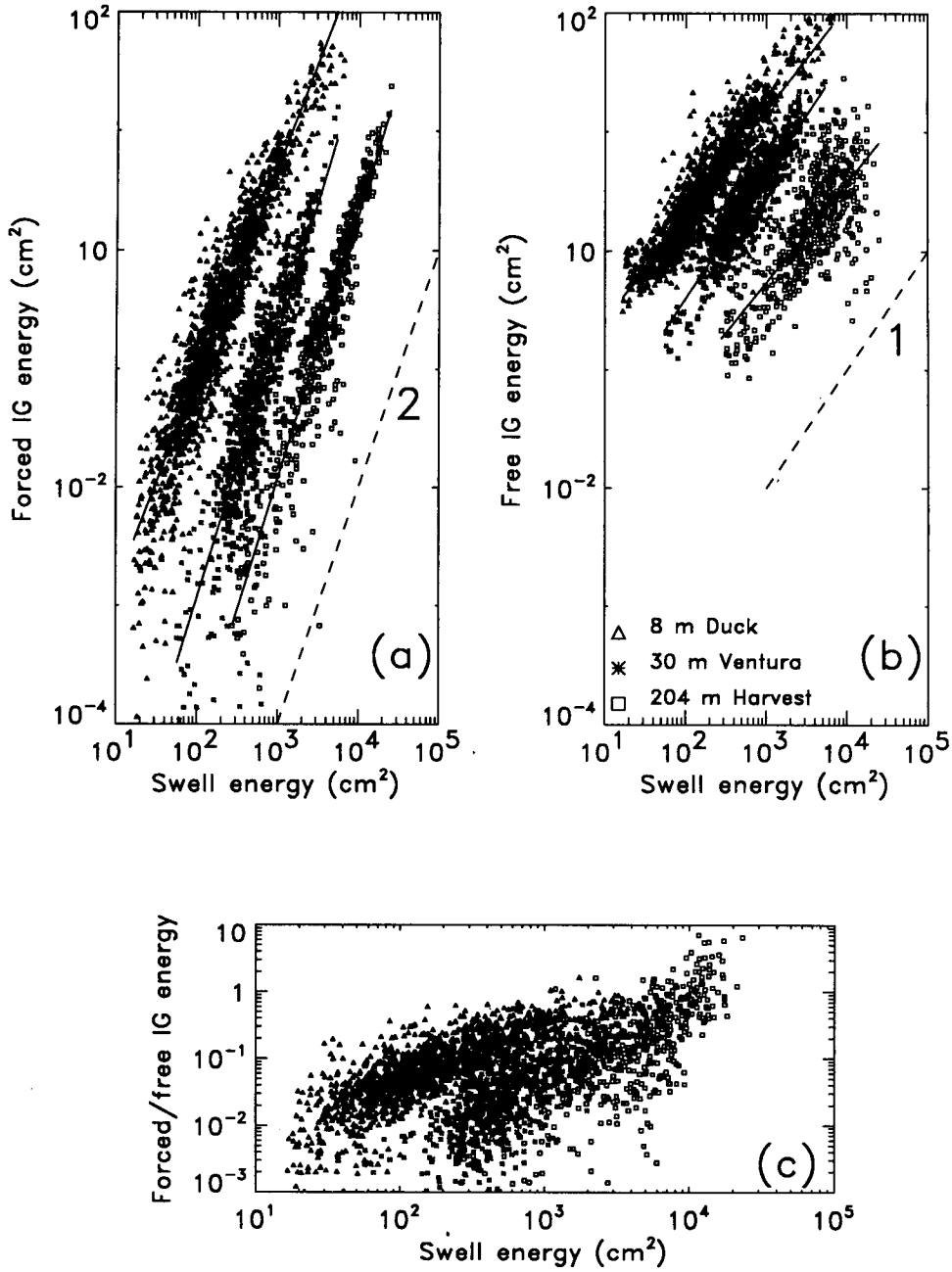

FIG. 4. (a) Forced infragravity energy, (b) free infragravity energy, and (c) the ratio of forced to free infragravity energy versus swell energy. Infragravity energies were integrated over the frequency ranges 0.004–0.05 Hz and 0.004–0.04 Hz in the Atlantic and Pacific, respectively. The data are from 8 m depth at Duck (triangles, upper clouds), 30 m at Ventura (asterisks, middle clouds), and 204 m at Harvest Platform (squares, lower clouds). The solid lines are least-squares-fit curves to the logarithms of the observed energies. Dashed lines labeled 1 and 2 indicate linear and quadratic dependencies, respectively.

The observed ratios of forced to free infragravity energy range between 10^{-3} and 10 (Fig. 4c), indicating that either free or forced waves can dominate the infragravity band. Owing to the different dependencies of free and forced wave energies on swell energy and water depth (e.g., cf. Figs. 4a and 4b), the relative contribution of forced waves to the infragravity band energy increases with both increasing swell energy and decreasing water depth. Overall, the present observations (including the sites not shown in Fig. 4) indicate that free waves are the dominant source of infragravity energy on the shelf (outside the surf zone), although

forced wave contributions are significant in shallow water and can even dominate the infragravity band in deeper water when the swell is very energetic. (Note the forced/free wave energy ratios > 1 for swell energy > 10^4 cm^2 in 204-m depth in Fig. 4c.)

Although the observed decrease of free infragravity energy with increasing water depth h (Fig. 4b) is not inconsistent with theoretical propagation effects, these observations were obtained at different sites. Thus, differences in free infragravity energy may have resulted from the different wind wave climates or geographic surroundings (see section 5), as well as from the different depths. The seabed between the simultaneously sampled gauges in 8-m and 13-m depth at Duck was nearly planar, and thus, the effect of alongshore depth variations on wave propagation between these measurement locations is small. According to linear long-wave theory, the energy of nonbreaking free waves propagating perpendicular to a gently sloping beach with no alongshore depth variations is proportional to $h^{-1/2}$ (e.g., Eckart 1951). The decrease in total (free plus forced) infragravity energy levels observed between 8 and 13 m depth at Duck was previously shown to be close to the theoretical $h^{-1/2}$ value (0.78) for leaky free waves when incident swell energy levels were very low, and to increase systematically with increasing swell energy (Fig. 3 in Elgar et al. 1992). This trend was attributed to increasing forced wave contributions (with a strong depth dependence) to the infragravity band with increasing swell energy.

The present bispectral decomposition of infragravity energy into free and forced wave contributions allows an assessment of the depth dependence of free wave energy. The ratio R of 13-m to 8-m depth free infragravity wave energy observed at Duck is approximately independent of swell energy (Fig. 5), confirming that the trend of increased R (based on the total infragravity energy) with energetic swell observed by Elgar et al. (1992) is indeed caused by forced wave contributions. In fact, the largest free wave R values occur with very low swell energy, less than 30 cm^2 (discussed in section 6). Although the observed values of R vary between 0.4 and 1, the majority are in the range 0.5–0.7, lower than the theoretical value $R > 0.78$ for leaky waves (leaky wave obliquity increases R above the 0.78 value for shore-normal propagation; e.g., Kinsman 1965). The R values of 0.5–0.7 suggest that a significant fraction (10%–50%) of the free infragravity energy radiated seaward in 8-m depth is refracted back toward shore at a turning point between 8-m and 13-m depth.

According to Snell's law, only free long waves traveling seaward at angles greater than 52° (relative to the beach-normal) in 8-m depth are refracted back toward the beach between 8-m and 13-m depth. Hence, the observed variation in free wave energy between 8-m and 13-m depth implies that a substantial fraction of free wave energy in these depths propagates at large angles relative to the beach-normal. Array measurements in 13-m depth confirm that free infragravity waves are directionally broad with significant alongshore propagation (Fig. 6). The estimation procedure (Herbers and Guza 1990) assumes a free wave field that is spatially homogeneous across the array. Free waves dominated the cases shown in Fig. 6, and the cross-spectra were smoothed over wide (0.007 Hz) frequency bands, thus effectively eliminating the spatial inhomogeneities associated with standing waves (apparent in the high-resolution spectra in Fig. 3a).

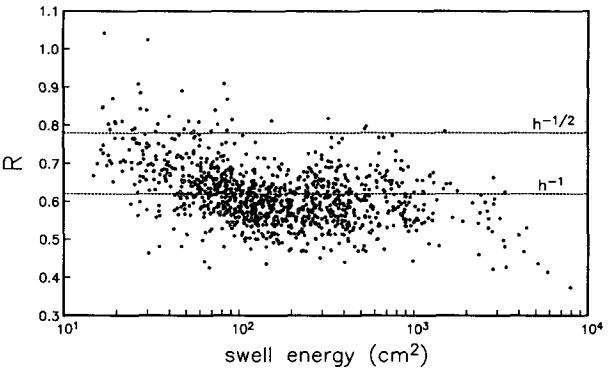

FIG. 5. The ratio R of free infragravity energy in 13-m depth to that in 8-m depth versus incident swell energy (in 13-m depth) at Duck. Dotted lines indicate the theoretical $h^{-1/2}$ variation for leaky waves propagating in a direction perpendicular to the depth contours, and the stronger h^{-1} dependence predicted for an isotropic directional spectrum.

The directional distribution of infragravity wave energy apparently depends on the directional properties of swell. For example, when the directionally narrower, onshore propagating swell was traveling upcoast (90° < θ < 180°), infragravity waves were also traveling predominantly upcoast (0° < θ < 180°, Figs. 6a,b). Similarly, when the swell was traveling downcoast (180° < θ < 270°, Fig. 6c), downcoast (180° < θ < 360°) propagating infragravity waves were observed. With normally incident swell the peak of the infragravity spectrum is directed offshore (Fig. 6d). Similar trends were previously observed at Duck in 8-m depth (Oltman-Shay 1991). The energy of seaward traveling infragravity waves is about a factor 2 larger than the energy of shoreward traveling infragravity waves for the cases shown in Fig. 6, an imbalance possibly caused by energy dissipation on the shelf (see Elgar et al. 1994 for further discussion). A detailed analysis of the dependence of infragravity wave directional properties on incident swell conditions, based on the entire 9-month long dataset, will be given in a subsequent publication.

4. Geometrical optics-continuum model

Geometrical optics (WKB) theory is now used to show that the observed cross-shore variation of free infragravity wave energy (Fig. 5) is qualitatively con-

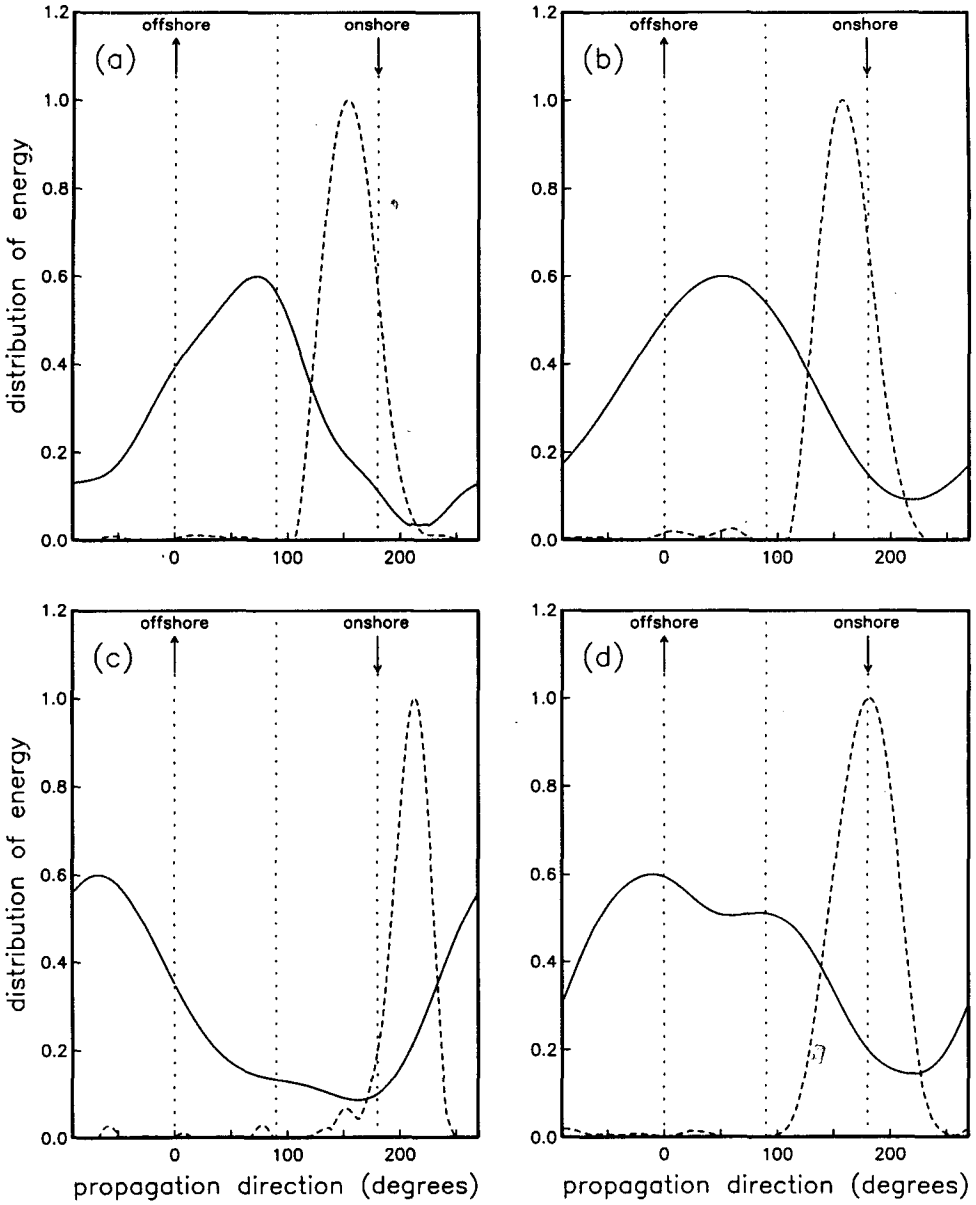

FIG. 6. Directional distributions of frequency band-integrated infragravity (solid lines) and swell (dashed lines) energy estimated from array measurements in 13-m depth at Duck. Dates of observation and the corresponding swell variances are (a) 11 October 1990: 551 cm^2, (b) 13 October 1990: 1366 cm^2, (c) 30 November 1990: 721 cm^2, and (d) 24 February 1991, 386 cm^2.

sistent with the refractive trapping of a directionally broad spectrum of long waves. Owing to multiple, constructively interfering reflections between the shoreline and offshore turning points, the infragravity energy radiated from shore may be concentrated in discrete edge wave modes. A plane beach with constant slope β extending to deep water supports edge wave modes with alongshore wavenumbers

$$k_y = \frac{(2\pi f)^2}{g \sin[(2n+1)\beta]}, \quad (2n+1)\beta < \frac{\pi}{2}, \quad (1)$$

where f is the edge wave frequency, n is the mode number, and g is gravity (Ursell 1952). Analytic edge wave solutions are known for other idealized topographies (e.g., Ball 1967; Longuet-Higgins 1967) and edge wave solutions to the shallow water equations can be obtained numerically for arbitrary, smooth cross-shore depth variations (e.g., Holman and Bowen 1979). WKB solutions can be obtained for edge waves on smooth bathymetry with both cross-shore and alongshore depth variations (e.g., Shen et al. 1968). WKB solutions for progressive waves are not valid near

the shoreline nor offshore turning points, where the associated singularities are eliminated by heuristically introducing reflected waves (appendix A). Schäffer and Jonsson (1992) show that for mode numbers $n > 2$ the WKB approach yields edge wave dispersion relations close to the exact solutions for both plane [Eq. (1)] and exponential (Ball 1967) beach profiles. Although previous studies have shown that a significant fraction of the infragravity energy in the surf zone is contained in lower mode ($n \leq 2$) edge waves (e.g., Huntley et al. 1981; Oltman-Shay and Guza 1987), these motions do not extend very far offshore. For 0.02-Hz waves on a beach with slope $\beta = 0.01$ (roughly equivalent to the Duck inner shelf), only modes $n > 5$ reach 8-m depth, and these higher-mode edge waves are well described by a WKB approximation (appendix A).

The wavenumber separation of adjacent edge wave modes decreases as the mode number n increases [Eq. (1)]. Hence, adjacent high-mode edge waves on a gently sloping seabed are expected to be approximately equally excited (unless the infragravity forcing is very narrowbanded). Additionally, as n increases, the distance between the shoreline and the offshore turning point increases (e.g., Eckart 1951), and scattering from topographic irregularities on the shelf will tend to equalize energy in adjacent edge wave modes. Therefore, the edge wave energy far from shore should vary smoothly from mode to mode and is conveniently approximated by an equivalent continuum, analogous to the Garrett and Munk (1972, 1975) model for vertical internal wave modes.

In the shallow water WKB approximation, the directional spectrum $E(\theta; x)$ of free infragravity waves radiating from shore on a gently (monotonically) sloping seabed $h = h(x)$ with no alongshore depth variations is given by (e.g., Longuet-Higgins 1957; Le Méhauté and Wang 1982)

$$E(\theta; x) = \frac{h_s}{h(x)} E(\theta_s(\theta; x); x_s) \quad \text{for} \quad -\frac{\pi}{2} < \theta < \frac{\pi}{2}, \quad (2)$$

where x_s (with depth h_s) is a location shoreward of x and the propagation direction θ_s at x_s is given by Snell's law

$$\theta_s(\theta; x) = \arcsin\left[\left(\frac{h_s}{h(x)}\right)^{1/2} \sin\theta\right]. \quad (3)$$

At x_s, only waves traveling seaward with propagation directions θ_s within the aperture

$$-\alpha(x) < \theta_s < \alpha(x); \quad \alpha(x) = \arcsin\left[\left(\frac{h_s}{h(x)}\right)^{1/2}\right] \quad (4)$$

reach a distance x offshore. Waves propagating seaward with larger oblique angles ($|\theta_s| > \alpha$) are refractively trapped between x_s and x. In the WKB shallow water approximation, waves propagating obliquely seaward (i.e., $\theta \neq 0$) at location x are specularly reflected from offshore turning points and the directional spectrum of shoreward traveling waves at x is given by

$$E(\theta; x) = E(\pi - \theta; x) \quad \text{for} \quad \frac{\pi}{2} < \theta < \pi \quad \text{and} \quad \pi < \theta < \frac{3\pi}{2}. \quad (5)$$

The directional spectrum of free infragravity waves $E(\theta; x)$ is isotropic if the spectrum close to shore $E(\theta_s; x_s)$ is white for seaward propagation angles in the range $-\alpha < \theta_s < \alpha$ [Eqs. (2), (4), (5)]. For the asymptotic case where x is far offshore of x_s and $h(x) \gg h_s$, the aperture $\alpha(x) \approx [h_s/h(x)]^{1/2}$ is very small, and $E(\theta; x)$ is directionally isotropic for any directionally smooth radiation of infragravity wave energy from shore. Integration of Eqs. (2) and (5) over θ yields an asymptotic h^{-1} dependence of free infragravity energy.

The asymptotic WKB limit is compared to simulations of a discrete spectrum of edge wave modes on a plane seabed with slope $\beta = 0.01$ in Fig. 7. The edge wave energy prediction $E(x)$ (also based on shallow water equations, Eckart 1951) was obtained by summing the variances of a large number of edge wave modes within a narrow ($\Delta f = 0.004$ Hz) frequency band centered at $f = 0.02$ Hz

$$E(x) = \sum_{m=-M/2}^{M/2} \sum_{n=1}^{N} \frac{E_n}{M+1} \times [\exp(-k_y^{n,m} x) L_n(2k_y^{n,m} x)]^2, \quad (6)$$

where $k_y^{n,m}$ is the alongshore wavenumber of edge wave mode n with frequency $f + (m\Delta f)/M$ [appendix A, Eqs. (A7), (A9)], and E_n is the shoreline variance of mode n (assumed white across the frequency bandwidth Δf). Results are shown for three hypothetical shoreline energy distributions (Fig. 7a), corresponding to radiation that is approximately isotropic, weighted toward shore-normal propagation (i.e., relatively energetic high modes), and weighted toward oblique propagation (i.e., relatively energetic low modes). Although the cross-shore variations of edge wave energy near the shoreline differ, reflecting the relative weighting of low modes, for offshore distances greater than a few kilometers all cases agree well with the asymptotic h^{-1} rolloff predicted by WKB theory (Fig. 7b). The edge wave spectra 5 km from shore in 50-m depth are in good agreement with the directionally isotropic spectrum predicted by WKB theory (Fig. 7c; the transformation of an isotropic $E(\theta)$ to k_y space is described in appendix B). Other choices of shoreline energy distributions that are smooth at high mode numbers yield similar results; the offshore distance required to reach the theoretical asymptotic limit is not large.

As shown in appendix B and Fig. 7c, a directionally isotropic spectrum ($E(\theta) = \text{const}$) corresponds to an

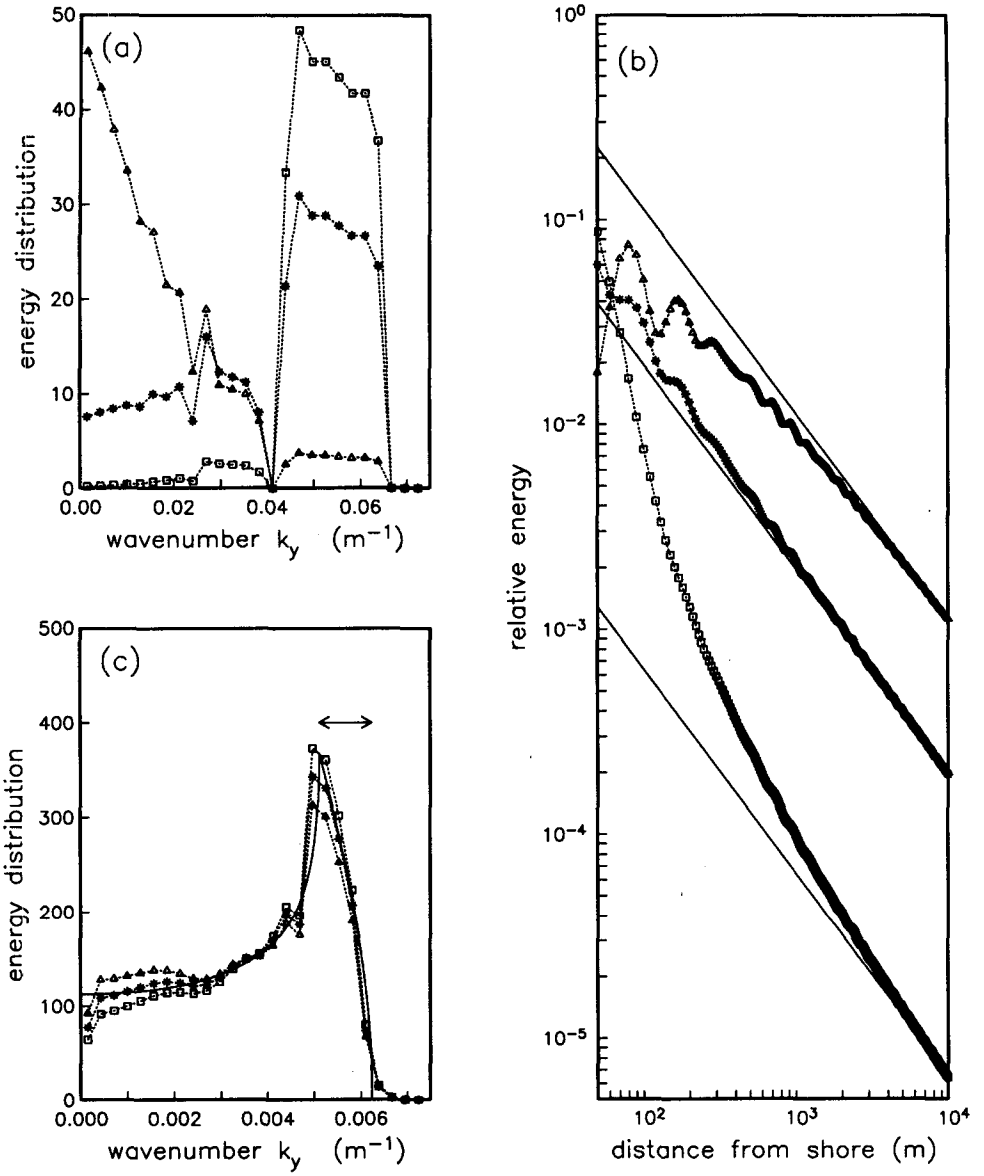

FIG. 7. Properties of a spectrum of edge waves [Eq. (6), for large N, M] on a plane seabed with slope $\beta = 0.01$ (Eckart 1951) are compared to an asymptotic WKB approximation for three hypothetical mode mixes. (a) Shoreline energy distributions as a function of the alongshore wavenumber k_y (symmetric about $k_y = 0$). Mode mixes are of the form $E_n \propto n^{-2} \exp[\gamma/n]$ with $\gamma = 0$ (asterisks: corresponding to approximately isotropic radiation), $\gamma = -4$ (triangles: dominated by high modes), and $\gamma = 4$ (squares: dominated by low modes). (b) Edge wave energy (relative to the total edge wave energy at the shoreline) as a function of distance from shore. Symbols correspond to the different shoreline energy distributions shown in panel a. The asymptotic WKB h^{-1} variation is indicated by solid lines. (c) The distribution of edge wave energy as a function of alongshore wavenumber in 50-m depth, 5 km from shore. The WKB approximation (solid curve) corresponds to an isotropic directional spectrum [Eq. (B3); the caustic region $[k_1, k_2]$ is indicated by arrows].

alongshore wavenumber spectrum $E(k_y)$ with a maximum near the cutoff wavenumber k_{yc}

$$k_{yc}(x) = \frac{2\pi f}{(gh(x))^{1/2}} \tag{7}$$

corresponding to the lowest mode edge wave that has a turning point seaward of the cross-shore position x (e.g., Ball 1967; Longuet-Higgins 1967). This concentration of edge wave energy near the cutoff mode ($0.0051 < k_{yc} < 0.0062$ m^{-1} in Fig. 7c) is qualitatively consistent with estimates of $E(k_y)$ obtained by J. Oltman-Shay (1990, personal communication) in 8-m depth at Duck, and observed in the alongshore velocity field within the surf zone (Oltman-Shay and Guza 1987).

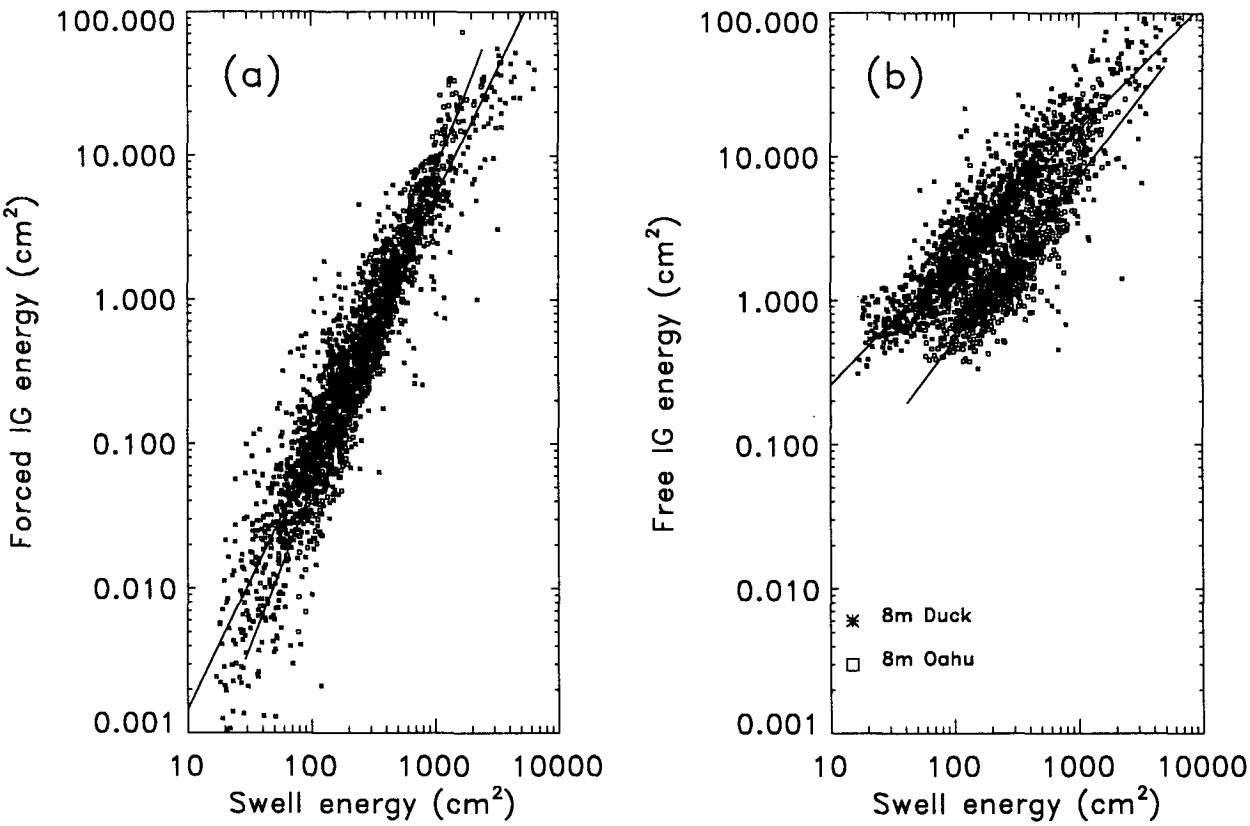

FIG. 8. (a) Forced and (b) free infragravity energies observed in 8-m depth at Duck (asterisks, upper cloud in Fig. 8b) and Oahu (squares, lower cloud) vs swell energy. Solid lines are least-squares-fit curves to the logarithms of the observed energies.

Although the observed ratios R between free infragravity wave energy in 13-m and 8-m depth at Duck generally agree better with the asymptotic h^{-1} dependence ($R = 0.62$) for a broad spectrum than with the $h^{-1/2}$ dependence ($R = 0.78$) for shore-normal propagating waves, there is considerable variability (Fig. 5). Similarly, the observed $E(\theta)$ of infragravity waves are broad (Fig. 6) but not isotropic (the asymptotic limit). Deviations from the asymptotic limit are not surprising since the measurements were obtained only 1–2 km from shore, and additional model assumptions of no alongshore depth variations and no radiation of infragravity energy to deep water (i.e., shallow water theory) are not realistic. However, the qualitative agreement of this simple, asymptotic continuum WKB model with both exact shallow water edge wave solutions (Fig. 7) and the observations (Fig. 5) is encouraging and suggests that an extended WKB approach may be useful in modeling the propagation of infragravity waves over continental shelves. Whereas exact edge wave solutions are difficult to obtain with finite and alongshore-variable depths, the approximate spectral WKB theory can be extended to include slowly varying two-dimensional shelf topographies and finite depth effects such as radiation to deep water. Furthermore, dissipation of infragravity energy on the shelf (Elgar et al. 1994) may be included in a spectral WKB model as a local sink term in the energy balance (e.g., Hasselmann and Collins 1968).

5. Effects of geographic surroundings

The similar dependence of forced wave energy on swell energy at different sites, but in the same water depth (Figs. 8a, 9a, 10a), confirms that forced waves are a local effect, independent of the surrounding beach and shelf topography. However, because free infragravity motions are refractively trapped during propagation over the shelf, and subsequently reflected from the beach face, their energy levels additionally depend on the larger-scale geographic surroundings (Figs. 8b, 9b, 10b). Free wave energy levels in 8-m depth at Oahu are typically lower by a factor of 2–4 than in the same depth at Duck with comparable swell energy (Fig. 8b). Some of these differences may result from the different Pacific and Atlantic wave climates (i.e., predominantly lower frequency swell at Oahu, Fig. 3a). However, swell conditions at both Oahu and Duck are quite variable [i.e., low-frequency swell occurs at Duck, and high-frequency swell at Oahu, see Fig. 1 in Elgar et al. (1992)], and yet there is little overlap between Duck and Oahu free infragravity wave energy levels. Gen-

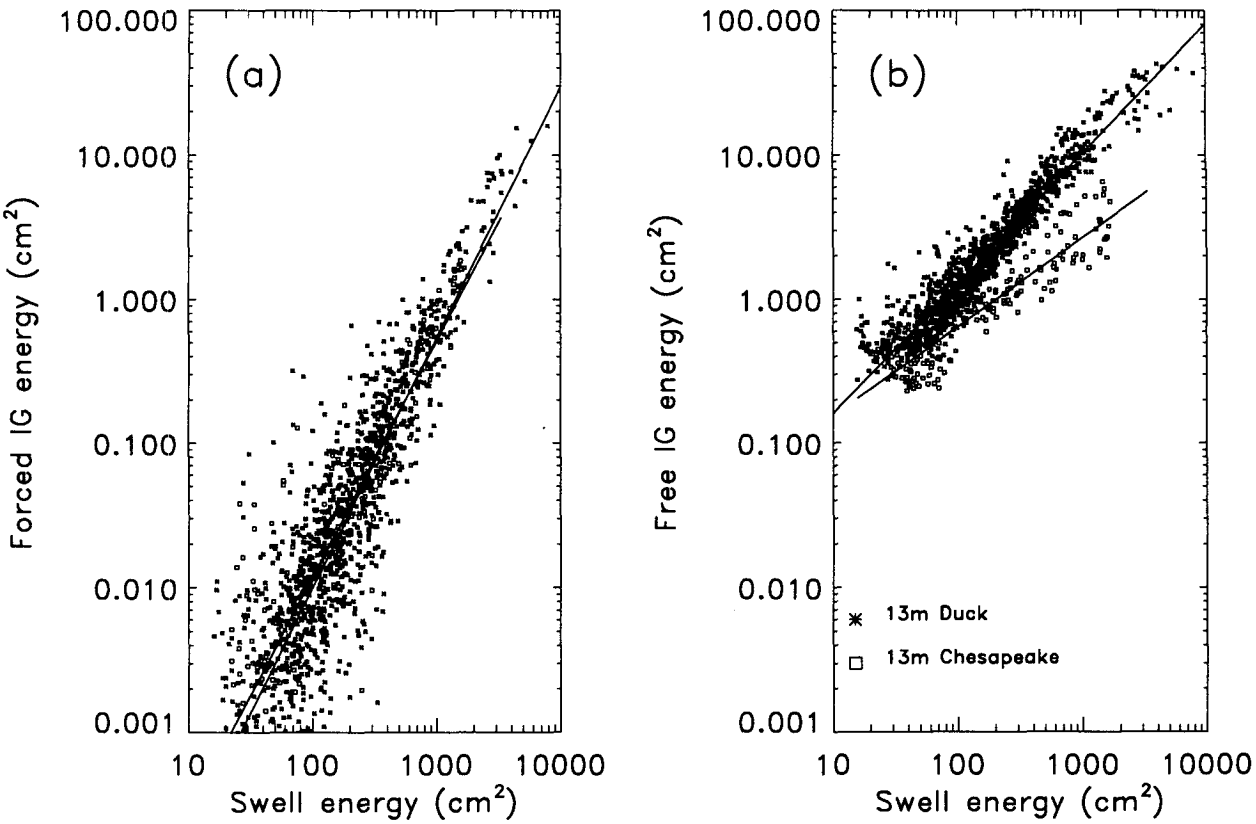

FIG. 9. (a) Forced and (b) free infragravity energies observed in 13-m depth at Duck (asterisks, upper cloud in Fig. 9b) and the Chesapeake Light Tower (squares, lower cloud) vs swell energy. Solid lines are least-squares-fit curves to the logarithms of the observed energies.

eration of free waves may be sensitive to the beach profile, but both the Oahu and Duck gauges were situated approximately 1 km offshore of similarly sloped beaches. Although the Duck and Oahu beaches are similar, the shelves are very different. At Duck a gently sloping, shallow (depths < 50 m) shelf extends approximately 80 km from shore, whereas offshore of Oahu the depth increases rapidly to 200 m within 1 km from shore (Figs. 1, 2). This large difference in shelf widths may strongly affect the refractive trapping of free waves. As the slope of the seabed increases, there are fewer possible edge wave modes. For example, a plane beach with slope $\beta = 1°$ supports 45 edge wave modes, whereas only the Stokes mode $n = 0$ exists for $\beta > 30°$ [Eq. (1)]. Additionally, as β increases, the k_y range that supports edge waves is reduced. Thus, the narrow Oahu shelf may be less efficient than the broad Duck shelf at trapping infragravity waves radiating from shore, consistent with the observed difference in energy levels. The relative differences between Oahu and Duck infragravity energy levels decrease with increasing swell energy (Fig. 8b), possibly because the efficiency with which infragravity energy is refractively trapped and reflected on the Duck shelf is significantly reduced by dissipation during storms. This interpretation is consistent with the observed increase of the ratio between seaward and shoreward propagating infragravity energy in 13-m depth at Duck from roughly 1–2 for moderate swell conditions (e.g., Fig. 6) to 3–4 for energetic swell conditions (Elgar et al. 1994).

Free infragravity energy levels observed in 13-m depth at the Chesapeake Light Tower are consistently lower than observed in 13-m depth at Duck (Fig. 9b). The sites, located on the same broad shelf offshore of mildly sloping sandy beaches, are separated by only about 100 km in the alongshelf direction (Fig. 1a). However, the 13-m Duck site is 2 km from shore, whereas the light tower is situated on a shoal about 25 km from shore (Fig. 2). Free waves radiating from shore at relatively large oblique angles that reach the Duck gauge are refractively trapped by slightly deeper waters (19 m) shoreward of the Chesapeake shoal, resulting in lower infragravity energy levels at the Chesapeake Light Tower. However, the proximity to Chesapeake Bay may also reduce infragravity energy levels at the light tower owing to the absence of a surf zone across the bay mouth. Dissipation of free infragravity waves propagating over the 25 km of relatively shallow water separating the light tower from shore is also possibly significant. The observed divergence of the Duck and Chesapeake Light Tower infragravity energy levels with increasing swell energy (Fig. 9b) is consistent with

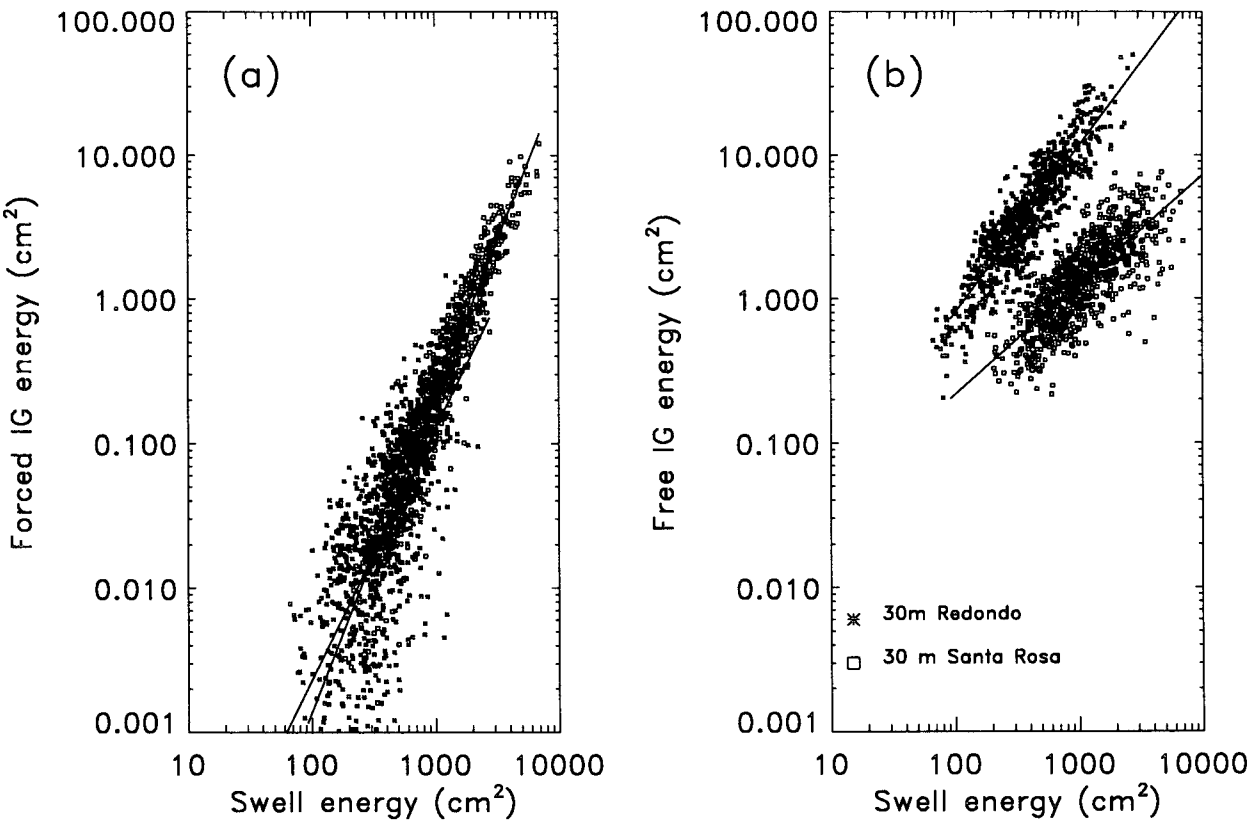

FIG. 10. (a) Forced and (b) free infragravity energies observed in 30-m depth at Redondo (asterisks, upper cloud in Fig. 10b) and Santa Rosa Island (squares, lower cloud) vs swell energy. Solid lines are least-squares-fit curves to the logarithms of the observed energies.

increased nonlinear dissipation on the shelf reducing the amount of seaward radiated energy reaching the light tower. A similar trend is observed in the ratio of energies in 8-m and 13-m depth at Duck (Fig. 5). When swell energy is high the free infragravity energy in 13-m depth is reduced relative to that in 8-m depth.

A more dramatic difference in free infragravity energy levels was observed between the southern California stations in 30-m depth at Redondo and Santa Rosa Island (Fig. 10b). For similar incident swell conditions, energy levels observed at Santa Rosa were typically an order of magnitude lower than at Redondo. Differences in shelf topography affect the propagation and trapping of free waves and thus may cause these different infragravity energy levels. However, variations in free wave energy levels observed at a large number of southern California coastal locations in 30-m depth (including the Redondo and Ventura stations, Fig. 1b) are much smaller than the differences observed between Redondo and Santa Rosa, even though the shelf topography between the coastal stations varies appreciably (i.e., cf. the shelf profile at Ventura to those near Redondo and Santa Rosa, Fig. 2). Similarly, free infragravity wave energy levels at other 30-m depth stations on the south and west side of Santa Rosa Island are comparable to the (north) Santa Rosa observations shown in Fig. 10b and much lower than the coastal energy levels. The beaches (where the free infragravity motions are believed to be generated) around Santa Rosa Island are markedly different from those on the mainland shelf, with steep cliffs and shallow reefs near Santa Rosa Island and gentle slopes near the coastal stations. Concomitant differences in shoreline reflections and localized breaking of incident swell, which affect nonlinear shoaling and surf zone processes, may explain the observed differences in free infragravity energy levels.

6. Arrival from remote sources

At the seafloor in deep ocean basins, forced infragravity energy is negligible owing to attenuation over the water column. The primary source of infragravity energy is the weak radiation to deep water of free infragravity waves from coasts where incident swell (and infragravity wave) energy levels are high (Webb et al. 1991). The present observations show that this background radiation from distant shores is the dominant source of infragravity energy on the shelf when generation by local swell is extremely weak. For the relatively few cases with very low energy swell (variances less than 30 cm^2), the observed ratio R between free infragravity energy in 13-m and 8-

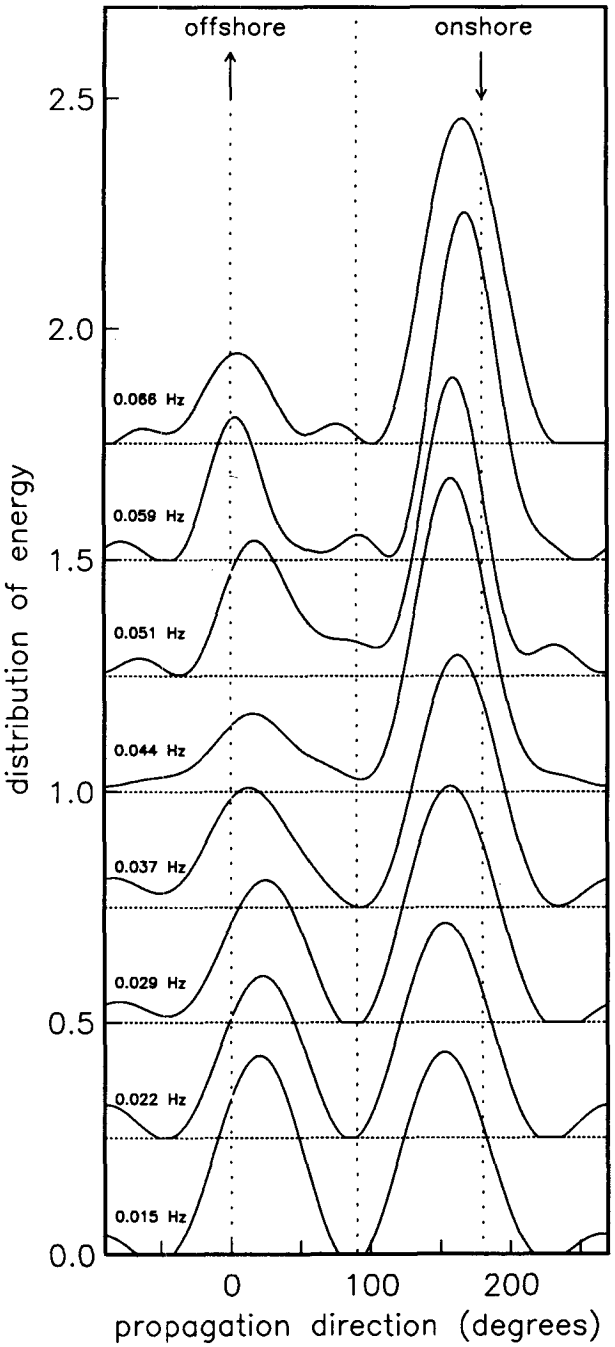

FIG. 11. Directional distributions of energy at infragravity frequencies observed in 13-m depth at Duck on 17 November 1990 when the local swell energy was very low (18 cm^2). The distribution at each frequency is normalized to unit area and the curves are offset for clarity.

m depth at Duck is usually larger than for cases with energetic swell, and closer to the theoretical value $R = 0.78$ for leaky waves (Fig. 5).

Directional distributions of infragravity wave energy observed in 13-m depth when local swell energy levels were very low (Fig. 11 and other examples not shown) are consistent with infragravity waves arriving from the deep ocean and reflecting from the beach. The distributions are bimodal with relatively narrow peaks at seaward and shoreward propagation directions (Fig. 11), in contrast to the broader directional distributions with significant alongshore propagation observed with more typical swell energies (Fig. 6). Also in contrast to observations with more energetic swell, the energy of shoreward traveling infragravity waves exceeds the energy of seaward traveling infragravity waves, indicating that energy arriving from deep water is dissipated and/or refractively trapped close to shore.

7. Conclusions

Motions in the infragravity frequency band (nominally 0.005–0.05 Hz) on the continental shelf are a mix of forced waves, phase coupled to wind waves, and free waves usually generated at nearby shores. Observed forced wave energy levels are accurately predicted by second-order nonlinear theory (see Part I), but the generation and subsequent propagation of free waves is poorly understood. The observed mix of forced and free waves is highly variable with the relative contribution of forced waves to the infragravity energy generally increasing with both increasing swell energy and decreasing water depth (Fig. 4).

Owing to multiple reflections between the shoreline and offshore turning points, free infragravity wave energy radiated from shore may be concentrated in discrete edge wave modes. Low-mode edge waves (sometimes important in the surf zone) do not reach far offshore, and high-mode edge wave energy is expected to vary smoothly with mode number on a low-slope seabed, owing to the small wavenumber separation of adjacent modes. In this case, a field of discrete edge wave modes may be approximated by a continuous directional spectrum. Shallow water WKB theory predicts that asymptotically far from shore, on a mildly and monotonically sloping seabed with no alongshore depth variations, free infragravity wave spectra are directionally isotropic with energy levels inversely proportional to the water depth h (Fig. 7). This asymptotic result is independent of the detailed directional structure of the infragravity wave field radiated from shore. Observed free infragravity energy levels in 8-m and 13-m depth, 1 and 2 km from shore, respectively, are qualitatively consistent with the predicted asymptotic h^{-1} variation (Fig. 5). Preliminary directional analysis shows that the infragravity wave field in 13-m depth is directionally broad, although the detailed directional structure at this site relatively close to shore is still quite variable and sensitive to incident swell directional properties (Fig. 6). The approximately h^{-1} dependence and broad directional distributions show that refractive trapping is of O(1) importance to free infragravity waves radiated from shore.

Energy levels of free infragravity waves on the shelf depend on the surrounding topography. For example, infragravity energy levels observed on a narrow shelf are significantly lower (about a factor 2-4, Fig. 8b) than those observed in the same depth on a broad shelf with similar incident swell conditions, possibly because narrow shelves trap less energy than broad shelves. Furthermore, energy levels observed offshore of a rocky coast are about an order of magnitude lower than those observed offshore of a sandy beach (Fig. 10b), probably because free infragravity wave radiation depends on the characteristics of the nonlinear shoaling and/or breaking of waves very close to shore. The dynamics are not understood, and further observations are needed, but the present analysis suggests that the shelf-wide topography is important to the propagation and trapping of free infragravity motions, whereas the generation and reflection of free infragravity waves is sensitive to the shoreline morphology.

Acknowledgments. This research was sponsored by the Office of Naval Research (Coastal Sciences and Nonlinear Ocean Waves Accelerated Research Initiative) and the California Department of Boating and Waterways. The 13-m depth Virginia, 13-m depth North Carolina, and 30-m depth California pressure sensors were deployed by the staff of the Center for Coastal Studies, Scripps Institution of Oceanography. The 8-m depth North Carolina data were collected by the U.S. Army Corps of Engineers Field Research Facility, Coastal Engineering Research Center, Duck, North Carolina. The 8-m depth Oahu and 204-m depth Harvest Platform data, graciously provided by M. Okihiro and R. Seymour, were collected by the Coastal Data Information Program (supported by the U.S. Army Corps of Engineers and the California Department of Boating and Waterways). We thank A. Bowen for helpful discussions and C. Winant for making his workstation available for 14 621 bispectral calculations.

APPENDIX A

WKB-Geometrical Optics Approximation of Edge Waves

The WKB-geometrical optics approximation of edge waves is illustrated with a simple example of edge waves in shallow water on a plane beach with slope β

$$h(x, y) = x \tan\beta. \tag{A1}$$

The surface elevation function $\eta_+(x, y, t)$ of a seaward propagating wave component with wavenumber $\mathbf{k} = [k_x, k_y]$ can be expressed in the WKB shallow water approximation as (e.g., Friedrichs 1948):

$$\eta_+(x, y, t) = Ax^{-1/4}\left[\frac{k}{k_x}\right]^{1/2} \times \cos\left(\int_0^x dx k_x + k_y y - \sigma t + \Phi_+\right), \tag{A2}$$

where A and Φ_+ are an arbitrary wave amplitude and phase, respectively; t is time; and the radian frequency σ ($=2\pi f$) is given by the shallow water dispersion relation

$$\sigma = (gh)^{1/2}k; \quad k = |\mathbf{k}|. \tag{A3}$$

At the caustic x_c where k_x vanishes [Eqs. (A1), (A3)],

$$x_c = \frac{\sigma^2}{k_y^2 g \tan\beta}, \tag{A4}$$

a reflected wave with the same amplitude A and alongshore wavenumber k_y, and a phase Φ_- is introduced

$$\eta_-(x, y, t) = Ax^{-1/4}\left[\frac{k}{k_x}\right]^{1/2} \times \cos\left(-\int_0^x dx k_x + k_y y - \sigma t + \Phi_-\right). \tag{A5}$$

Asymptotically matching the combined wave profile

$$\eta(x, y, t) = \eta_+(x, y, t) + \eta_-(x, y, t) = 2Ax^{-1/4}\left[\frac{k}{k_x}\right]^{1/2} \cos\left(\int_0^x dx k_x + \frac{\Phi_+ - \Phi_-}{2}\right) \times \cos\left(k_y y - \sigma t + \frac{\Phi_+ + \Phi_-}{2}\right) \tag{A6}$$

to exact standing wave solutions near the shoreline (with unit amplitude at $x = 0$; Friedrichs 1948) and near the caustic (e.g., Chao 1971) yields the (exact) shallow water edge wave dispersion relation (e.g., Schäffer and Jonsson 1992)

$$k_y = \frac{\sigma^2}{g(2n + 1)\tan\beta}; \quad n = 0, 1, 2, 3, \cdots \tag{A7}$$

and the WKB edge wave surface elevation profile

$$\eta(x, y, t) = [(2n + 1)\pi]^{-1/2}[x'(1 - x')]^{-1/4} \times \cos\left((2n + 1)\left[[x'(1 - x')]^{1/2} - \frac{1}{2}\arcsin(1 - 2x') + \frac{\pi}{4}\right] - \frac{\pi}{4}\right)\cos(k_y y - \sigma t + \Phi) \quad 0 < x < x_c, \tag{A8}$$

where $x' \equiv x/x_c$ and $\Phi \equiv \Phi_+ + \pi/4$. The ray paths of a few low mode edge waves in the WKB approximation [Eq. (A8)] are shown in Fig. A1a, and the good agreement with exact (Eckart 1951) shallow water solutions

$$\eta(x, y, t) = \exp(-k_y x)L_n(2k_y x)\cos(k_y y - \sigma t + \Phi) \tag{A9}$$

is illustrated in Fig. A1b.

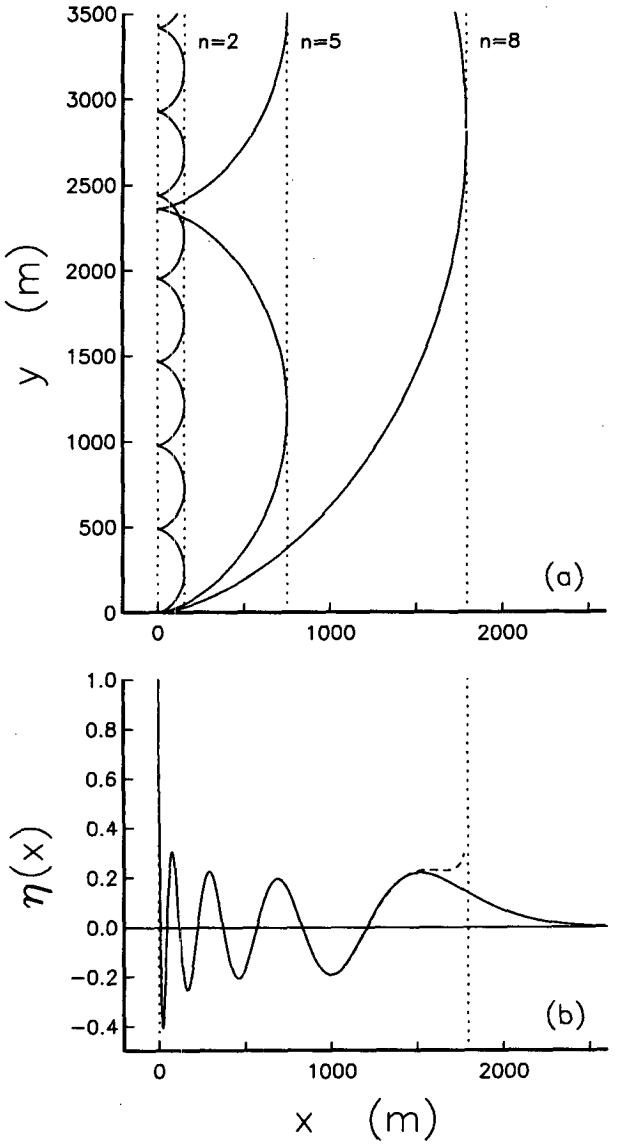

FIG. A1. Shallow water WKB approximation of 0.02-Hz edge waves on a plane beach with slope $\beta = 0.01$. (a) Ray trajectories for modes 2, 5, and 8. (b) Sea surface elevation versus offshore distance for mode 8. Solid and dashed curves correspond to the exact solution [Eq. (A9); Eckart 1951] and the WKB approximation [Eq. (A8)], respectively. Vertical dotted lines indicate the shoreline and caustic locations, where the singular WKB solution is not shown.

APPENDIX B

Wavenumber and Directional Spectra

Consider a frequency–directional spectrum $E(\sigma, \theta)$ white in both frequency and direction within a frequency band $[\sigma_1, \sigma_2]$

$$E(\sigma, \theta) = E; \quad \sigma_1 < \sigma < \sigma_2, \quad 0 \leq \theta < 2\pi. \quad \text{(B1)}$$

The corresponding frequency–alongshore wavenumber spectrum $E(\sigma, k_y)$ is given by

$$E(\sigma, k_y) = \begin{cases} \dfrac{2E}{(k^2 - k_y^2)^{1/2}} & \text{for} \quad |k_y| < k \\ 0 & \text{for} \quad |k_y| > k, \end{cases} \quad \text{(B2)}$$

with k the wavenumber given by the shallow water dispersion relation [Eq. (A3)]. Integration of $E(\sigma, k_y)$ [Eq. (B2)] over the frequency band $[\sigma_1, \sigma_2]$ yields

$$E(k_y) = \int_{\sigma_1}^{\sigma_2} d\sigma E(\sigma, k_y)$$

$$= \begin{cases} 2E(gh)^{1/2} \ln\left(\dfrac{k_2 + (k_2^2 - k_y^2)^{1/2}}{k_1 + (k_1^2 - k_y^2)^{1/2}}\right) \\ \quad \text{for} \quad |k_y| < k_1 \\ 2E(gh)^{1/2} \ln\left(\dfrac{k_2 + (k_2^2 - k_y^2)^{1/2}}{k_y}\right) \\ \quad \text{for} \quad k_1 < |k_y| < k_2 \\ 0 \quad \text{for} \quad |k_y| > k_2, \end{cases} \quad \text{(B3)}$$

with k_1 and k_2 the shallow water wavenumbers [Eq. (A3)] corresponding to frequencies σ_1 and σ_2, respectively. The spectrum $E(k_y)$ is maximum for $|k_y| = k_1$ (Fig. 7c).

REFERENCES

Ball, F. K., 1967: Edge waves in an ocean of finite depth. *Deep-Sea Res.*, **14**, 79–88.

Beardsley, R. C., H. Mofjeld, M. Wimbush, C. N. Flagg, and J. A. Vermersch Jr., 1977: Ocean tides and weather-induced bottom pressure fluctuations in the Middle-Atlantic Bight. *J. Geophys. Res.*, **82**, 3175–3182.

Bowen, A. J., and R. T. Guza, 1978: Edge waves and surf beat. *J. Geophys. Res.*, **83**, 1913–1920.

Chao, Y.-Y., 1971: An asymptotic evaluation of the wave field near a smooth caustic. *J. Geophys. Res.*, **76**, 7401–7408.

Chapman, D. C., and G. S. Giese, 1990: A model for the generation of coastal seiches by deep-sea internal waves. *J. Phys. Oceanogr.*, **20**, 1459–1467.

Eckart, C., 1951: Surface waves on water of variable depth. Wave Rep. 100, Scripps Institution of Oceanography, University of California, La Jolla, 99 pp.

Elgar, S., T. H. C. Herbers, M. Okihiro, J. Oltman-Shay, and R. T. Guza, 1992: Observations of infragravity waves. *J. Geophys. Res.*, **97**, 15 573–15 577.

——, ——, and R. T. Guza, 1994: Reflection of ocean surface gravity waves from a natural beach. *J. Phys. Oceanogr.*, **24**, 1503–1511.

Evans, D. V., 1988: Mechanisms for the generation of edge waves over a sloping beach. *J. Fluid Mech.*, **186**, 379–391.

Foda, M. A., and C. C. Mei, 1981: Nonlinear excitation of long-trapped waves by a group of short swells. *J. Fluid Mech.*, **111**, 319–345.

Friedrichs, K. O., 1948: Water waves on a shallow sloping beach. *Commun. Proc. Appl. Math.*, **1**, 109.

Gallagher, B., 1971: Generation of surf beat by non-linear wave interactions. *J. Fluid Mech.*, **49**, 1–20.

Garrett, C. J. R., and W. H. Munk, 1972: Space–time scales of internal waves. *Geophys. Fluid Dyn.*, **2**, 225–264.

——, and ——, 1975: Space–time scales of internal waves: A progress report. *J. Geophys. Res.*, **80**, 291–297.

Giese, G. S., D. C. Chapman, P. G. Black, and J. A. Fornshell, 1990: Causation of large-amplitude coastal seiches on the Caribbean coast of Puerto Rico. *J. Phys. Oceanogr.*, **20,** 1449–1458.

Greenspan, H. P., 1956: The generation of edge waves by moving pressure distributions. *J. Fluid Mech.*, **1,** 574–592.

Guza, R. T., and E. B. Thornton, 1985: Observations of surf beat. *J. Geophys. Res.*, **90,** 3161–3172.

Hasselmann, K., 1962: On the non-linear energy transfer in a gravity-wave spectrum. Part 1: General theory. *J. Fluid Mech.*, **12,** 481–500.

——, and J. I. Collins, 1968: Spectral dissipation of finite-depth gravity waves due to turbulent bottom friction. *J. Mar. Res.*, **26,** 1–12.

——, W. Munk, and G. MacDonald, 1963: Bispectra of ocean waves. *Times Series Analysis,* M. Rosenblatt, Ed., John Wiley, 125–139.

Herbers, T. H. C., and R. T. Guza, 1990: Estimation of directional wave spectra from multicomponent observations. *J. Phys. Oceanogr.*, **20,** 1703–1724.

——, and ——, 1991: Wind wave nonlinearity observed at the sea floor. Part I: Forced-wave energy. *J. Phys. Oceanogr.*, **21,** 1740–1761.

——, S. Elgar, and R. T. Guza, 1994: Infragravity-frequency (0.005–0.05 Hz) motions on the shelf. Part I: Forced waves. *J. Phys. Oceanogr.*, **24,** 917–927.

Holman, R. A., and A. J. Bowen, 1979: Edge waves on complex beach profiles. *J. Geophys. Res.*, **84,** 6339–6346.

——, D. A. Huntley, and A. J. Bowen, 1978: Infragravity waves in storm conditions. *Proc. 16th Conf. on Coastal Engineering,* New York, NY, Amer. Soc. Civ. Eng., 268–284.

Howd, P. J., J. Oltman-Shay, and R. A. Holman, 1991: Wave variance partitioning in the trough of a barred beach. *J. Geophys. Res.*, **96,** 12 781–12 795.

Huntley, D. A., R. T. Guza, and E. B. Thornton, 1981: Field observations of surf beat. Part 1: Progressive edge waves. *J. Geophys. Res.*, **86,** 6451–6466.

Kinsman, B., 1965: *Wind Waves: Their Generation and Propagation on the Ocean Surface.* Prentice-Hall, 676 pp.

Le Méhauté, B., and J. D. Wang, 1982: Wave spectrum changes on a sloped beach. *J. Waterw., Port, Coastal Ocean Eng.*, **108,** 33–47.

List, J. H., 1992: A model for the generation of two-dimensional surf beat. *J. Geophys. Res.*, **97,** 5623–5636.

Longuet-Higgins, M. S., 1957: On the transformation of a continuous spectrum by refraction. *Proc. Camb. Phil. Soc.*, **53,** 226–229.

——, 1967: On the trapping of wave energy round islands. *J. Fluid Mech.*, **29,** 781–821.

——, and R. W. Stewart, 1962: Radiation stress and mass transport in surface gravity waves with application to "surf beats." *J. Fluid Mech.*, **13,** 481–504.

Miller, G. R., W. H. Munk, and F. E. Snodgrass, 1962: Long-period waves over California's continental borderland. Part 2: Tsunamis. *J. Mar. Res.*, **20,** 31–41.

Morison, M. L., and J. Imberger, 1992: Water-level oscillations in Esperance Harbour. *J. Waterw., Port, Coastal Ocean Eng.*, **118,** 352–367.

Munk, W. H., 1949: Surf beats. *Eos Trans. Amer. Geophys. Union,* **30,** 849–854.

——, F. Snodgrass, and G. Carrier, 1956: Edge waves on the continental shelf. *Science,* **123,** 127–132.

Okihiro, M., R. T. Guza, and R. J. Seymour, 1992: Bound infragravity waves. *J. Geophys. Res.*, **97,** 11 453–11 469.

Oltman-Shay, J., 1991: A climatological study of infragravity waves in 8 meters depth. *Eos Trans. Amer. Geophys. Union,* **72,** 253.

——, and R. T. Guza, 1987: Infragravity edge wave observations on two California beaches. *J. Phys. Oceanogr.*, **17,** 644–663.

O'Reilly, W. C., R. T. Guza, B. W. Waldorf, M. R. Kirk, W. A. Boyd, and M. C. Clifton, 1992: Data report, Southern California Wave Experiment. Scripps Institution of Oceanography, Ref. Ser. No. 92-14, 89 pp.

Roelvink, J. A., H. A. H. Petit, and J. K. Kostense, 1992: Verification of a one-dimensional surfbeat model against laboratory data. *Proc. 23d Conf. on Coastal Engineering,* New York, NY, Amer. Soc. Civ. Eng., 960–973.

Schäffer, H. A., 1993: Infragravity waves induced by short-wave groups. *J. Fluid Mech.*, **247,** 551–588.

——, and I. A. Svendsen, 1988: Surf beat generation on a mild slope beach. *Proc. 21st Conf. on Coastal Engineering,* New York, NY, Amer. Soc. Civ. Eng., 1058–1072.

——, and I. G. Jonsson, 1992: Edge waves revisited. *Coastal Eng.*, **16,** 349–368.

——, ——, and I. A. Svendsen, 1990: Free and forced cross-shore long waves. *Water Wave Kinematics,* A. Torum and O. T. Gudmestad, Eds., Kluwer Academic, 367–385.

Seymour, R. J., M. H. Sessions, and D. Castel, 1985: Automated remote recording and analysis of coastal data. *J. Waterw., Port, Coastal Ocean Eng.*, **111,** 388–400.

Shen, M. C., R. E. Meyer, and J. B. Keller, 1968: Spectra of water waves in channels and around islands. *Phys. Fluids,* **11,** 2289–2304.

Shillington, F. A., 1984: Long period edge waves off Southern Africa. *Contin. Shelf Res.*, **3,** 343–357.

——, and D. van Foreest, 1986: Numerical model studies of long-period edge waves. *J. Phys. Oceanogr.*, **16,** 1487–1492.

Snodgrass, F. E., W. H. Munk, and G. R. Miller, 1962: Long-period waves over California's continental borderland. Part 1. Background spectra. *J. Mar. Res.*, **20,** 3–30.

Suhayda, J. N., 1974: Standing waves on beaches. *J. Geophys. Res.*, **79,** 3065–3071.

Symonds, G., D. A. Huntley, and A. J. Bowen, 1982: Two-dimensional surf beat: Long wave generation by a time-varying breakpoint. *J. Geophys. Res.*, **87,** 492–498.

Tucker, M. J., 1950: Surf beats: Sea waves of 1 to 5 minute period. *Proc. Roy. Soc. London, Ser. A,* **202,** 565–573.

Ursell, F., 1952: Edge waves on a sloping beach. *Proc. Roy. Soc. London, Ser. A,* **214,** 79–97.

Van Dorn, W. G., 1984: Some tsunami characteristics deducible from tide records. *J. Phys. Oceanogr.*, **14,** 353–363.

Webb, S. C., X. Zhang, and W. Crawford, 1991: Infragravity waves in the deep ocean. *J. Geophys. Res.*, **96,** 2723–2736.

Wright, L. D., R. T. Guza, and A. D. Short, 1982: Dynamics of a high-energy dissipative surf zone. *Mar. Geol.*, **45,** 41–62.